https://doi.org/10.1016/j.engstruct.2023.116983

Design-oriented stress-strain model for FRP-confined engineered cementitious composites

Shuai Li, Tak-Ming Chan*, Ben Young

Department of Civil and Environmental Engineering, The Hong Kong Polytechnic University, Hong Kong, China

*Corresponding author. *Email address:* tak-ming.chan@polyu.edu.hk (T.-M. Chan).

Abstract

Engineered cementitious composites (ECC) is known for its enhanced tensile performance compared with normal concrete. Ductile strain hardening behavior, multiple cracking beahvior as well as large tensile strain capacity can be achieved for ECC under tensile loadings. For the compressive performance, using lateral fiber-reinforced polymer (FRP) confinement is an effective approach to improve the compressive strength and strain. However, the research work on design models of FRP-confined ECC, especially on the stress-strain relationship, is limited at the current stage. To address this aspect, this study focuses on developing the design-oriented stress-strain model for FRP-confined ECC under axial compression. A test database on FRP-confined ECC was firstly assembled. Existing design equations on FRP-confined concrete were evaluated and found not be able to provide satisfactory predictions for FRP-confined ECC. New design equations on ultimate conditions, including the ultimate compressive strength and ultimate axial strain, were then proposed and verified with the test results. Finally, the design-oriented stress-strain model for FRP-confined ECC was developed, which consists of the formulated form of a stress-strain model for FRP-confined normal concrete and the new design equations on ultimate conditions proposed for FRP-confined ECC. Predictions of stress-strain curve show close agreements with test results, indicating the good performance of the developed design-oriented stress-strain model.

Keywords: Engineered cementitious composites (ECC); Fiber-reinforced polymer (FRP); Confinement; Compressive behavior; Design-oriented model

1. Introduction

Engineered cementitious composites (ECC) is gaining increasing popularity in recent years as an advanced cementitious material [1-3]. Compared with normal concrete, ECC has short polymer fibers distributed in the mixture to improve the tensile behavior [4]. It demonstrates a strain-hardening tensile stress-strain relationship with significantly enhanced ultimate tensile strain of up to 10% [5], as shown in Fig. 1(a). Due to the fiber-bridging effect through the microcracks, the width of tensile cracks in ECC can be controlled and prevented from continuing growing, which leads to the multiple cracking behavior [6]. With the good ductility and toughness, ECC has been adopted in different structural members for various structural rehabilitation purposes, such as avoiding large tensile cracks and protecting steel rebars in the tensile zone in reinforced concrete beams [7-8], providing additional lateral confinement to the core concrete in hybrid columns [9-11] as well as strengthening the plastic hinge zone of beam-column joints [12,13]. These applications show that with limited amount of normal concrete replaced by ECC in the structural member, targeted improvement of the structural performance can be achieved. Meanwhile, the durability of structures with ECC cover can be increased as well, since the inner steel reinforcement are protected from corrosion with the good crack width control ability of ECC. It is cost-effective from the life cycle perspective.

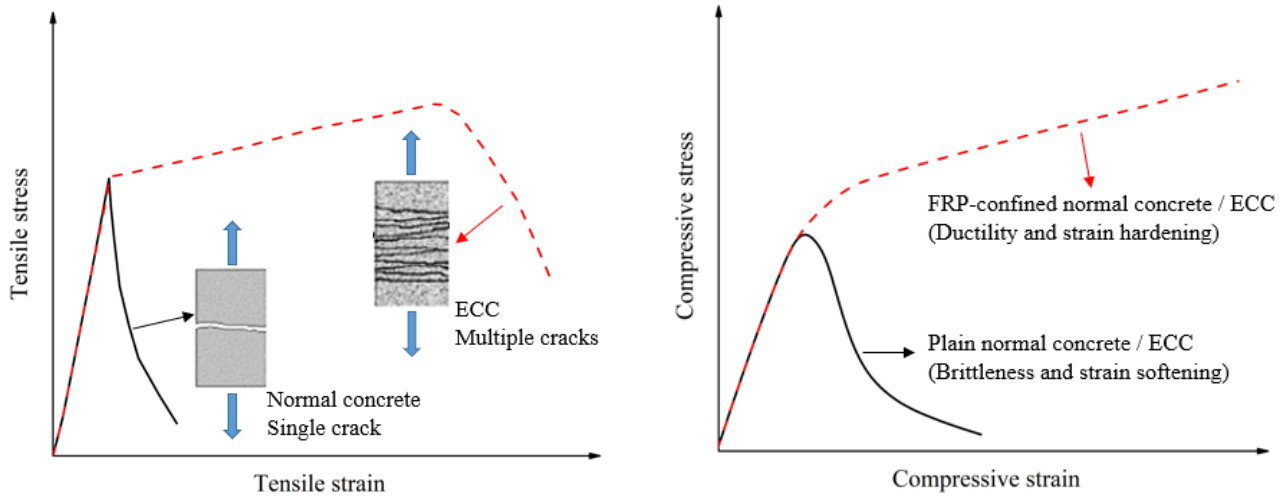

(a) Tensile behavior (b) Compressive behavior

Fig. 1 Tensile and compressive behavior of normal concrete and ECC

Similar to normal concrete, ECC also presents the brittleness and strain softening behavior at the post-peak stage. In order to improve the compressive behavior of ECC, researchers noted that adopting lateral fiber-reinforced polymer (FRP) confinement is an effective approach like FRP-confined normal concrete, as shown in Fig. 1(b). Dang et al. [14] compared the axial compressive behavior of ECC cylinders and normal concrete cylinders confined by FRP jackets. It was found that the ultimate conditions corresponding to FRP rupture failure could be effectively enhanced with lateral FRP confinement for both FRP-confined normal concrete and FRP-confined ECC. However, the deformability of FRP-confined ECC was 10% - 78% larger than that of FRP-confined normal concrete with similar unconfined strength and confinement level. Li et al. [15] carried out tests on FRP-confined ECC under both monotonic and cyclic axial compressions and noted that uniform hoop strain distribution could be obtained due to the multiple cracking behavior of ECC. It could avoid the premature FRP rupture caused by localized concrete cracking and lead to improved ultimate conditions. Meanwhile, the FRP rupture failure could be delayed with further enhanced ultimate compressive strength and ultimate axial strain for FRP-confined ECC under cyclic compression, compared with that under monotonic compression. A similar behavior has also been observed for FRP-confined normal concrete [16,17]. Yuan et al. [18] analyzed the lateral dilation behavior of FRP-confined ECC and reported that the lateral strain development was lower compared with that of normal concrete due to the restraint effect caused by fibers in ECC mixture. Subsequently, appropriate lateral strain-axial strain model for FRP-confined ECC under axial compression was developed and verified. Li et al. [15] proposed the first analysis-oriented model for FRP-confined ECC, which was shown to be able to provide close predictions on the compressive stress-strain curves through defining the relations among axial stress, axial strain, lateral strain and lateral confining pressure. In these existing studies [14,15,18], it is also noted that the compressive strain corresponding to the peak stress for plain ECC is larger than that of plain normal concrete with similar compressive strength, which also leads to the phenomenon that ECC can present the larger compressive deformability. ECC has also been used together with

normal concrete to form the hybrid column under FRP confinement for achieving enhanced structural performance. Li et al. [19] proposed a novel composite column, in which an ECC layer is added between outer FRP tube and inner high strength concrete (HSC) core. It was found that the ECC layer could redistribute the localized hoop strain from HSC core to FRP tube to realize a more uniform hoop strain distribution on the FRP tube. Therefore, the column premature failure caused by HSC brittleness was eased or prevented and the deformability and ductility of the composite column were improved [19]. Finite element approach and design recommendations considering the different FRP confinement effect caused by the ECC layer in this novel composite column have also been developed accordingly [20-22]. Based on these existing studies, it can be noted that FRP-confined ECC has the potential to exhibit advantages over FRP-confined normal concrete in terms of the deformability performance. FRP-confined ECC could be considered under extreme conditions, such as seismic loadings where the structural members are required to withstand relatively large deformations. Meanwhile, hybrid use of ECC and normal concrete is also possible. With limited amount of normal concrete replaced by ECC in crucial regions of structural members, the structural behavior will be effectively improved with limited cost increase. For composite columns with the hybrid use of ECC and normal concrete, the ECC proportion is usually relatively low. The stiffness of the composite columns with ECC is similar to that of the counterpart columns without ECC, though the elastic modulus of ECC is lower than that of normal concrete [11,19].

Compared to FRP-confined normal concrete, studies on FRP-confined ECC are still relatively limited, especially on the reliable design approaches. Design equations on ultimate compressive strength and ultimate axial strain of FRP-confined ECC were developed based on the obtained test results [14,23]. However, these equations show deviations with each other. In the ultimate compressive strength equation, for example, Dang et al. [14] adopted 2.5 as the strength enhancement factor, while Yuan et al. [23] adopted 2.34 as the strength enhancement factor and assigned an additional size effect factor. These design equations could only provide acceptable predictions for their own test results. Meanwhile,

design-oriented model which can directly describe the compressive stress-strain behavior of FRP-confined ECC is not available in the existing research. Design-oriented models consisting of closed-form equations are developed through regression analyses and are calibrated from axial compression test results of FRP-confined concrete. The accuracy of these models depends greatly on the size and reliability of the test database as well as the parametric range of the test data used in the model development. Meanwhile, the compressive properties of ECC and normal concrete are different, especially that lateral dilation of ECC can be further restrained due to the fibers in ECC mixture as reported in Yuan et al. [18]. These indicate that design-oriented models developed for FRP-confined normal concrete may not be applicable to FRP-confined ECC. Therefore, this study will focus on developing the design-oriented stress-strain model for FRP-confined ECC. A test database on FRP-confined ECC was firstly collected based on literature in this study. Existing representative design equations on the ultimate conditions were then evaluated for FRP-confined ECC, and corresponding new equations were proposed. Design-oriented stress-strain model incorporating the new proposed design equations on the ultimate conditions of FRP-confined ECC was finally developed and verified with the test curves.

2. Database for FRP-confined ECC

In this section, 46 test results on FRP-confined ECC were collected in the literature to form the database as presented in Table 1. Specimen details are illustrated in Fig. 2. Different specimen sizes, FRP types, FRP thicknesses and ECC strengths are covered in the database. All the specimens are stub columns and have the height-to-diameter ratio of 2 with the diameter ranging from 100 mm to 500 mm. Glass FRP (GFRP) and Carbon FRP (CFRP) with different tensile elastic moduli and thicknesses are included, which yields various lateral confinement levels. Different ECC mixtures with polyethylene (PE) or polyvinyl alcohol (PVA) fibers were adopted in the corresponding research. ECC compressive strength is in the range of 28.2 to 64.6 MPa. Ultimate conditions including ultimate compressive strength f'_{cu}, ultimate axial strain ε_{cu} and hoop rupture strain $\varepsilon_{h,rup}$ are summarized in

Table 1 for the collected specimens. Meanwhile, the corresponding actual lateral confining pressure $f_{lu,a}$, confinement stiffness ratio ρ_K and strain ratio ρ_ε are calculated with the following equations [33] and listed in Table 1.

$$f_{lu,a} = \frac{2E_f t_f \varepsilon_{h,rup}}{D} \tag{1}$$

$$\rho_K = \frac{K_l}{f'_{c0}/\varepsilon_{c0}} = \frac{2E_f t_f}{(f'_{c0}/\varepsilon_{c0})D} \tag{2}$$

$$\rho_\varepsilon = \frac{\varepsilon_{h,rup}}{\varepsilon_{c0}} \tag{3}$$

where D is the diameter of confined ECC; E_f and t_f are the elastic modulus and thickness of confining FRP; K_l is FRP confining stiffness; f'_{c0} and ε_{c0} are the compressive strength and the corresponding compressive strain of unconfined ECC. It should be noted that in *Refs*. [18] and [23], large rupture strain (LRS) FRPs, including polyethylene naphthalate (PEN) and polyethylene terephthalate (PET) FRPs, were also adopted as the confining materials to form the FRP-confined ECC stub columns. LRS FRPs present large rupture strains and typical bi-linear tensile stress-strain behavior. The elastic modulus of the first linear portion is larger than that of the second linear portion, which leads to the different lateral confining pressure versus hoop strain behavior for LRS FRP-confined concrete in comparison to conventional FRP-confined concrete. Therefore, the specimens with LRS FRP in *Refs*. [18] and [23] are not summarized in Table 1 and are not included in the scope of the current study.

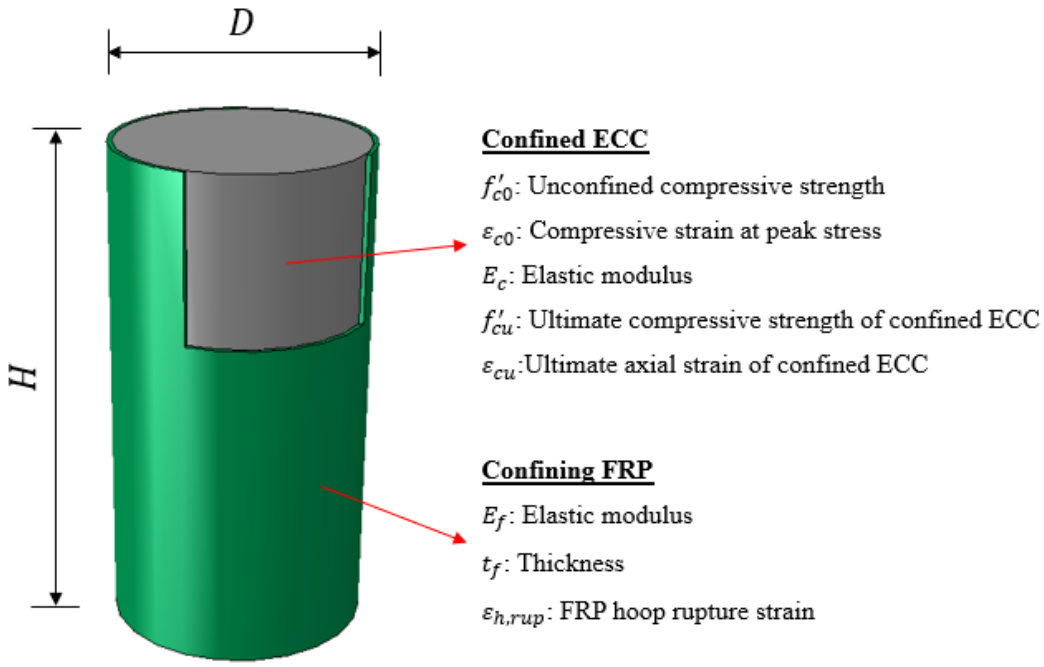

136

137 Fig. 2 Specimen details of FRP-confined ECC

138

Table 1 Database of test results on FRP-confined ECC

Source	Specimen label	Specimen Size		Specimen properties					Test results									
		D (mm)	H (mm)	FRP type	t_f (mm)	E_f (GPa)	f'_{c0} (MPa)	ε_{c0}	E_c (GPa)	f'_{cu} (MPa)	ε_{cu}	$\varepsilon_{h,rup}$	$f_{lu,a}$ (MPa)	ρ_K	ρ_ε	$\frac{f'_{cu}}{f'_{c0}}$	$\frac{\varepsilon_{cu}}{\varepsilon_{c0}}$
Li et al. [15]	G-6-M1	100	200	GFRP	2.000	39.2	40.0	0.0041	15.0	99.2	0.0713	0.0180	28.22	0.161	4.390	2.480	17.390
	G-6-M2	100	200	GFRP	2.000	39.2	40.0	0.0041	15.0	105.2	0.0746	0.0188	29.48	0.161	4.585	2.630	18.195
	G-6-C	100	200	GFRP	2.000	39.2	40.0	0.0041	15.0	136.5	0.1025	0.0220	34.50	0.161	5.366	3.413	25.000
	G-8-M1	100	200	GFRP	2.450	39.2	40.0	0.0041	15.0	114.6	0.0815	0.0192	36.88	0.197	4.683	2.865	19.878
	G-8-M2	100	200	GFRP	2.450	39.2	40.0	0.0041	15.0	113.5	0.0849	0.0185	35.53	0.197	4.512	2.838	20.707
	G-8-C	100	200	GFRP	2.450	39.2	40.0	0.0041	15.0	113.3	0.0913	0.0190	36.50	0.197	4.634	2.833	22.268
	G-7-M1	200	400	GFRP	2.350	39.2	40.0	0.0041	15.0	56.9	0.0266	0.0119	10.96	0.094	2.902	1.423	6.488
	G-7-M2	200	400	GFRP	2.350	39.2	40.0	0.0041	15.0	60.0	0.0272	0.0123	11.33	0.094	3.000	1.500	6.634
	G-7-C	200	400	GFRP	2.350	39.2	40.0	0.0041	15.0	56.8	0.0332	0.0145	13.36	0.094	3.537	1.420	8.098
	G-10-M1	200	400	GFRP	3.450	39.2	40.0	0.0041	15.0	85.0	0.0518	0.0141	19.07	0.139	3.439	2.125	12.634
	G-10-M2	200	400	GFRP	3.450	39.2	40.0	0.0041	15.0	84.6	0.0493	0.0140	18.93	0.139	3.415	2.115	12.024
	G-10-C	200	400	GFRP	3.450	39.2	40.0	0.0041	15.0	84.6	0.0555	0.0149	20.15	0.139	3.634	2.115	13.537
	C-2-M1	100	200	CFRP	0.220	255.0	40.0	0.0041	15.0	73.2	0.0507	0.0178	19.97	0.115	4.341	1.830	12.366
	C-2-M2	100	200	CFRP	0.220	255.0	40.0	0.0041	15.0	77.1	0.0616	0.0182	20.42	0.115	4.439	1.928	15.024
	C-2-C	100	200	CFRP	0.220	255.0	40.0	0.0041	15.0	77.0	0.0587	0.0155	17.39	0.115	3.780	1.925	14.317
	C-4-M1	100	200	CFRP	0.440	255.0	40.0	0.0041	15.0	192.4	0.1410	0.0238	53.41	0.230	5.805	4.810	34.390
	C-4-M2	100	200	CFRP	0.440	255.0	40.0	0.0041	15.0	130.8	0.0937	0.0183	41.07	0.230	4.463	3.270	22.853
	C-4-C	100	200	CFRP	0.440	255.0	40.0	0.0041	15.0	198.5	0.1418	0.0228	51.16	0.230	5.561	4.963	34.585
Yuan et al. [18]	E-GFRP-1-a	150	300	GFRP	0.169	100.5	28.2	0.0044	10.1	31.7	0.0287	0.0202	4.57	0.035	4.591	1.123	6.523
	E-GFRP-1-b	150	300	GFRP	0.169	100.5	28.2	0.0044	10.1	32.5	0.0299	0.0208	4.71	0.035	4.727	1.152	6.795
	E-GFRP-2-a	150	300	GFRP	0.338	100.5	28.2	0.0044	10.1	44.0	0.0479	0.0205	9.28	0.071	4.659	1.559	10.886
	E-GFRP-2-b	150	300	GFRP	0.338	100.5	28.2	0.0044	10.1	45.0	0.0470	0.0235	10.64	0.071	5.341	1.595	10.682
	E-GFRP-3-a	150	300	GFRP	0.507	100.5	28.2	0.0044	10.1	54.8	0.0633	0.0224	15.22	0.106	5.091	1.942	14.386
	E-GFRP-3-b	150	300	GFRP	0.507	100.5	28.2	0.0044	10.1	55.4	0.0818	0.0262	17.80	0.106	5.955	1.963	18.591
Dang et al. [14]	E-G2-M	100	200	GFRP	0.338	91.1	64.6	0.0035	23.7	83.3	0.0171	0.0144	8.87	0.034	4.068	1.289	4.886
	E-G5-M	100	200	GFRP	0.845	91.1	64.6	0.0035	23.7	139.0	0.0395	0.0169	26.02	0.084	4.774	2.152	11.286
	E-G8-M	100	200	GFRP	1.352	91.1	64.6	0.0035	23.7	217.1	0.0561	0.0234	57.64	0.135	6.610	3.361	16.029
	E-C2-M	100	200	CFRP	0.222	236.9	64.6	0.0035	23.7	95.3	0.0147	0.0126	13.25	0.058	3.559	1.475	4.200
	E-C5-M	100	200	CFRP	0.555	236.9	64.6	0.0035	23.7	162.8	0.0351	0.0145	38.13	0.144	4.096	2.520	10.029
	E-C8-M	100	200	CFRP	0.888	236.9	64.6	0.0035	23.7	245.4	0.0707	0.0180	75.73	0.231	5.085	3.799	20.200

Yuan et al. [23]	100-G-1-a	100	200	GFRP	0.169	100.5	51.6	0.0027	22.6	61.6	0.0093	0.0159	5.40	0.018	5.889	1.194	3.444
	100-G-1-b	100	200	GFRP	0.169	100.5	51.6	0.0027	22.6	63.9	0.0101	0.0152	5.16	0.018	5.630	1.238	3.741
	100-G-2-a	100	200	GFRP	0.338	100.5	51.6	0.0027	22.6	83.7	0.0113	0.0144	9.78	0.036	5.333	1.622	4.185
	100-G-2-b	100	200	GFRP	0.338	100.5	51.6	0.0027	22.6	77.1	0.0109	0.0155	10.53	0.036	5.741	1.494	4.073
	200-G-2-a	200	400	GFRP	0.338	100.5	51.6	0.0027	22.6	59.0	0.0077	0.0170	5.77	0.018	6.296	1.143	2.852
	200-G-2-b	200	400	GFRP	0.338	100.5	51.6	0.0027	22.6	59.0	0.0091	0.0133	4.52	0.018	4.926	1.143	3.370
	200-G-4-a	200	400	GFRP	0.676	100.5	51.6	0.0027	22.6	78.9	0.0101	0.0170	11.55	0.036	6.296	1.529	3.741
	200-G-4-b	200	400	GFRP	0.676	100.5	51.6	0.0027	22.6	81.1	0.0163	0.0164	11.14	0.036	6.074	1.572	6.037
	300-G-3-a	300	600	GFRP	0.507	100.5	51.6	0.0027	22.6	61.6	0.0097	0.0160	5.44	0.018	5.926	1.194	3.593
	300-G-3-b	300	600	GFRP	0.507	100.5	51.6	0.0027	22.6	62.3	0.0093	0.0160	5.44	0.018	5.926	1.207	3.444
	300-G-6-a	300	600	GFRP	1.014	100.5	51.6	0.0027	22.6	73.6	0.0112	0.0160	10.87	0.036	5.926	1.426	3.148
	300-G-6-b	300	600	GFRP	1.014	100.5	51.6	0.0027	22.6	80.8	0.0117	0.0160	10.87	0.036	5.926	1.566	4.333
	400-G-4-a	400	800	GFRP	0.676	100.5	51.6	0.0027	22.6	59.6	0.0099	0.0160	5.44	0.018	5.926	1.155	3.667
	400-G-4-b	400	800	GFRP	0.676	100.5	51.6	0.0027	22.6	54.1	0.0094	0.0160	5.44	0.018	5.926	1.048	3.481
	500-G-5-a	500	1000	GFRP	0.845	100.5	51.6	0.0027	22.6	56.9	0.0094	0.0160	5.44	0.018	5.926	1.103	3.481
	500-G-5-b	500	1000	GFRP	0.845	100.5	51.6	0.0027	22.6	53.4	0.0095	0.0160	5.44	0.018	5.926	1.035	3.519

Note: D and H are the diameter and height of the specimen; t_f and E_f are the thickness and elastic modulus of the confining FRP; f'_{c0}, ε_{c0} and E_c are the compressive strength, the corresponding compressive strain and elastic modulus of the unconfined ECC; f'_{cu} and ε_{cu} are the ultimate compressive strength and ultimate axial strain of FRP-confined ECC at FRP rupture; $\varepsilon_{h,rup}$ is the FRP hoop rupture strain; $f_{lu,a}$ is the actual confining pressure at FRP rupture.

Table 2 Existing prediction models for compressive strain at peak stress ε_{c0} and elastic modulus E_c for unconfined concrete

Model	Compressive strain at peak stress ε_{c0}	Elastic modulus E_c (Unit in MPa)
Eurocode 2 [24]	$\varepsilon_{c0} = 0.0007 f_{c0}'^{0.31}$	$E_c = 22000(\frac{f'_{c0}}{10})^{0.3}$
AIJ [25]*	N.A.	$E_c = 21000(\frac{\gamma}{2300})^{1.5}(\frac{f'_{c0}}{20})^{0.5}$
ACI 318 [26]	N.A.	$E_c = 4730\sqrt{f'_{c0}}$
Popovic [27]	$\varepsilon_{c0} = 0.000937\sqrt[4]{f'_{c0}}$	N.A.
Lim and Ozbakkaloglu [28]	$\varepsilon_{c0} = \frac{f_{c0}'^{0.225}}{1000}(\frac{152}{D})^{0.1}(\frac{2D}{H})^{0.13}$	$E_c = 4400\sqrt{f'_{c0}}$
Tasdemir et al. [29]	$\varepsilon_{c0} = (-0.067 f_{c0}'^2 + 29.9 f'_{c0} + 1053) \times 10^{-6}$	N.A.
De Nicolo et al. [30]	$\varepsilon_{c0} = 0.00076 + \sqrt{(0.626 f'_{c0} - 4.33) \times 10^{-7}}$	N.A.

*Note: γ is concrete density with unit in kg/m^3.

146 The mechanical properties of ECC could be different from those of normal concrete due to the different
147 mixtures [14]. Fig. 3 shows the basic trend between compressive strength f'_{c0} and the corresponding
148 compressive strain at the peak stress ε_{c0} as well as elastic modulus E_c of unconfined ECC for the
149 collected data as presented in Table 1. It can be noted that with the increase of ECC compressive
150 strength, ε_{c0} will decrease while E_c will increase. In Table 2, it summarizes the existing equations for
151 ε_{c0} and E_c of normal concrete [24-30]. Predictions with these equations are presented in Fig. 3 for
152 unconfined ECC collected in the database with the compressive cylinder strengths of 28.2MPa, 40.0
153 MPa, 51.6 MPa and 64.6 MPa. For the strain at peak stress ε_{c0}, the predicted results are lower than the
154 test results as shown in Fig. 3(a). It indicates that the strain at peak stress of ECC is larger than that of
155 the normal concrete with the same compressive strength. This agrees with the behavior that ECC can
156 present larger deformability than normal concrete under compressive loadings [14,15,18]. It is also
157 observed in Fig. 3(a) that the predicted strain at peak stress will increase with the increase of
158 compressive strength, which is a typical behavior for unconfined normal concrete. However, this
159 behavior is not in line with the current collected test results of ε_{c0} for ECC. The above observations
160 indicate that the existing equations on the prediction of the strain at peak stress for normal concrete
161 may not be applicable to ECC. On the other hand, the materials used in ECC mixtures in the four
162 literatures [14,15,18,23] are different, which may also affect the compressive strain at the peak stress.
163 For the elastic modulus E_c, the predicted results are obviously higher than the test results as shown in
164 Fig. 3(b). Due to the absence of coarse aggregates in ECC mixture, the elastic modulus of ECC is
165 lower than that of the normal concrete with the same compressive strength [31,32]. Therefore, the
166 existing prediction equations of elastic modulus developed based on normal concrete are not applicable
167 to ECC as well. For the data presented in Table 1, the following linear expressions can be proposed:

168 $$\varepsilon_{c0} = -0.00003 f'_{c0} + 0.0052 \quad (4)$$

169 $$E_c = 397.83 f'_{c0} - 489.73 \quad (5)$$

in which the units of f'_{c0} and E_c are in MPa. It is noted that Eqs. (4) and (5) are only generated based on the collected test results to depict the basic trends of strain at peak stress and elastic modulus of ECC with different compressive strengths in the database as shown in Table 1. Similar to normal concrete, test database for ECC with various strengths need to be generated in future studies, to develop more comprehensive prediction models for the compressive strain at peak stress ε_{c0} and elastic modulus E_c. Meanwhile, Fig. 3 only aims to show the comparison of compressive properties between normal concrete and ECC with the same compressive strengths.

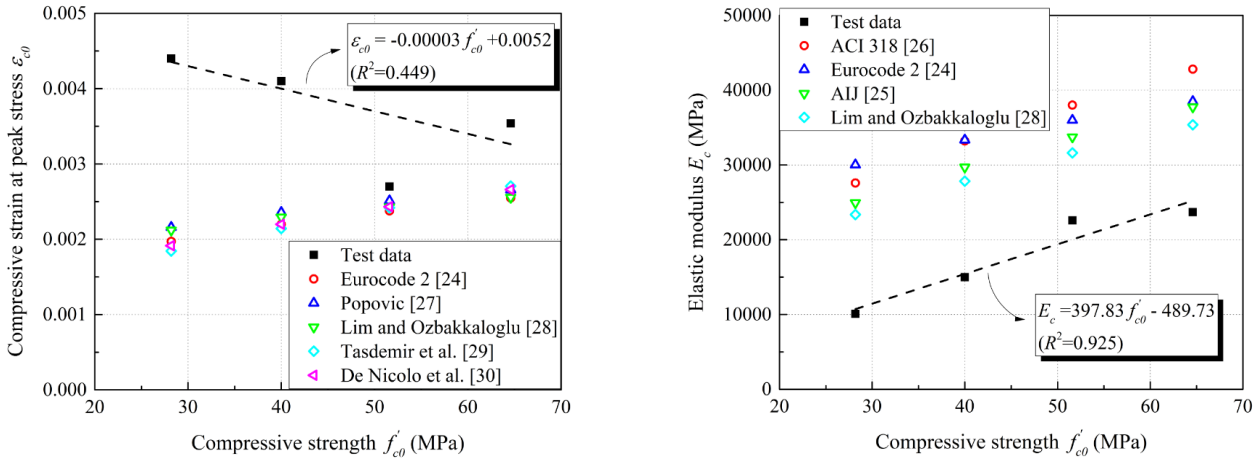

(a) Compressive strain at peak stress ε_{c0} (b) Elastic modulus E_c

Fig. 3 Compressive strain at peak stress ε_{c0} and elastic modulus E_c of unconfined ECC: collected test data and the corresponding predictions calculated by existing equations for normal concrete

3. Assessment of existing design equations on ultimate conditions

3.1 Existing models and assessment criterions

Ultimate conditions include ultimate compressive strength and ultimate axial strain corresponding to FRP rupture. They are the key parameters representing the compressive behavior of FRP-confined concrete. In this section, the existing design equations are assessed to observe their performance on FRP-confined ECC. As mentioned in the Introduction section, Dang et al. [14] and Yuan et al. [23] proposed the design equations on ultimate compressive strength and ultimate axial strain for FRP-

confined ECC based on their own obtained test data. These two sets of models are listed in Table 3 and used to conduct the assessment. Meanwhile, other representative design equations developed for FRP-confined normal concrete are also selected as presented in Table 3. Teng et al.'s model [33] could provide predictions for FRP-confined normal strength concrete (NSC) with good accuracy and has been adopted by the design codes [34,35]. Wei and Wu [36] proposed the models that were applicable to FRP-confined concrete columns with circular section, square and rectangular sections. Ozbakkaloglu and Lim [37] summarized a comprehensive database which covered a large range of parameters and developed the design equations on the ultimate conditions accordingly. Pour et al. [38] incorporated the test data for FRP-confined high strength concrete (HSC) and proposed the unified design model for both FRP-confined NSC and HSC. These models are widely accepted in the field of FRP-confined concrete [39,40]. Therefore, they are also selected to examine their performance on the prediction of FRP-confined ECC in this section.

Statistical indicators including mean (M), coefficient of variation (COV), average absolute error (AAE) and coefficient of determination (R^2) are employed to evaluate the accuracy of the predictions by different models, with the expressions given in the following Eqs. (6-9):

$$M = \frac{1}{n}\sum_{i=1}^{n}\frac{y_{test,i}}{y_{pred,i}} \tag{6}$$

$$COV = \frac{1}{M}\sqrt{\frac{\sum_{i=1}^{n}(\frac{y_{test,i}}{y_{pred,i}}-M)^2}{n-1}} \tag{7}$$

$$AAE = \frac{1}{n}\sum_{i=1}^{n}\left|\frac{y_{test,i}-y_{pred,i}}{y_{test,i}}\right| \tag{8}$$

$$R^2 = 1-\frac{\sum_{i=1}^{n}(y_{test,i}-y_{pred,i})^2}{\sum_{i=1}^{n}(y_{test,i}-\frac{1}{n}\sum_{i=1}^{n}y_{test,i})^2} \tag{9}$$

in which $y_{test,i}$ and $y_{pred,i}$ are the i^{th} test result and model predicted result, n is the total number of the test data in the database as presented in Table 1. If the values of M and R^2 are close to 1 and the values

of *COV* and *AAE* are close to 0, it demonstrates the good performance of the prediction model with higher accuracy and less scatterness.

3.2 Performance of the selected models

Comparisons between test results and predicted results for the ultimate conditions including normalized ultimate compressive strength f'_{cu}/f'_{c0} and normalized ultimate axial strain $\varepsilon_{cu}/\varepsilon_{c0}$ are presented in Fig. 4. In general, the predicted results deviate with the test results, indicating that the selected models present limited applicability on estimating the ultimate conditions of FRP-confined ECC. Statistical indicators for the different models are summarized in Table 4 and compared with each other in Fig. 5. For ultimate compressive strength, the models proposed by Teng et al. [33], Wei and Wu [36], Ozbakkaloglu and Lim [37], Dang et al. [14] and Yuan et al. [23] present the higher predictions by 3.1% - 15.4%. Pour et al.'s model [38] shows good average accuracy in terms of the mean value, while the *COV* value is relatively large and the R^2 value is lower than 0.9, which reveals the large scatterness between the predicted results and test results. For ultimate axial strain, all the selected models provide lower predictions, except that Teng et al.'s model [33] overestimates the results. Meanwhile, the large values of *COV* and *AAE* indicate that predictions by all the selected models scatter largely with the test results.

Table 3 Existing models for ultimate conditions of FRP-confined concrete

Model	Ultimate compressive strength	Ultimate axial strain
Teng et al. [33]	$\frac{f'_{cu}}{f'_{c0}} = 1 + 3.5(\rho_K - 0.01)\rho_\varepsilon$, if $\rho_K \geq 0.01$; $\frac{f'_{cu}}{f'_{c0}} = 1$, if $\rho_K < 0.01$	$\frac{\varepsilon_{cu}}{\varepsilon_{c0}} = 1.75 + 6.5\rho_K^{0.8}\rho_\varepsilon^{1.45}$
Wei and Wu [36]*	$\frac{f'_{cu}}{f'_{c0}} = 1 + 2.2(\frac{2r}{b})^{0.72}(\frac{f_{lu,a}}{f'_{c0}})^{0.94}(\frac{h}{b})^{-1.9}$	$\frac{\varepsilon_{cu}}{\varepsilon_{c0}} = 1.75 + 12\left(\frac{f_{lu,a}}{f'_{c0}}\right)^{0.75}\left(\frac{f'_{c30}}{f'_{c0}}\right)^{0.62}(0.36\frac{2r}{b} + 0.64)(\frac{h}{b})^{-0.3}$
Ozbakkaloglu and Lim [37]	$\frac{f'_{cu}}{f'_{c0}} = 1 + 0.0058\frac{K_l}{f'_{c0}} + 3.2\frac{(f_{lu,a} - K_l(0.43 + 0.009\frac{K_l}{f'_{c0}})\varepsilon_{c0})}{f'_{c0}}$	$\frac{\varepsilon_{cu}}{\varepsilon_{c0}} = 2 - \frac{(f'_{c0}-20)}{100} + 0.27(\frac{K_l}{f'_{c0}})^{0.9}\frac{\varepsilon_{h,rup}^{1.35}}{\varepsilon_{c0}}$, $2 - \frac{(f'_{c0}-20)}{100} \geq 1$
Pour et al. [38]	$\frac{f'_{cu}}{f'_{c0}} = 1 + (2.5 - 0.01f'_{c0})\frac{f_{lu,a}}{f'_{c0}}$	$\frac{\varepsilon_{cu}}{\varepsilon_{c0}} = 1.5 + (0.3 - 0.001f'_{c0})(\frac{K_l}{f'_{c0}})^{0.75}\frac{\varepsilon_{h,rup}^{1.35}}{\varepsilon_{c0}}$
Dang et al. [14]	$\frac{f'_{cu}}{f'_{c0}} = 1 + 2.5\frac{f_{lu,a}}{f'_{c0}}$	$\frac{\varepsilon_{cu}}{\varepsilon_{c0}} = 1.75 + 0.3\rho_\varepsilon + 13.94\rho_K\rho_\varepsilon$
Yuan et al. [23]	$\frac{f'_{cu}}{f'_{c0}} = \frac{1.18}{\sqrt{1+\frac{(H-D)}{394}}}(1 + 2.34\frac{f_{lu,a}}{f'_{c0}})$	N.A.

*Note: For square or rectangular section, r, b and h are the corner radius, length of the longer side and length of the shorter side, respectively. For circular section, r and b are the radius and diameter, respectively.

Table 4 Statistics of predictions on ultimate conditions by different models

Model	Ultimate compressive strength				Ultimate axial strain			
	M	COV	AAE	R^2	M	COV	AAE	R^2
Teng et al. [33]	0.866	0.139	0.190	0.649	0.952	0.286	0.310	0.936
Wei and Wu [36]	0.964	0.116	0.099	0.900	1.474	0.299	0.283	0.693
Ozbakkaloglu and Lim [37]	0.846	0.097	0.196	0.792	1.402	0.318	0.306	0.752
Pour et al. [38]	1.014	0.126	0.096	0.874	2.139	0.390	0.449	0.449
Dang et al. [14]	0.929	0.101	0.113	0.916	1.069	0.308	0.301	0.884
Yuan et al. [23]	0.969	0.109	0.102	0.924	-	-	-	-
Proposed models	**1.002**	**0.108**	**0.093**	**0.922**	**1.004**	**0.185**	**0.156**	**0.966**

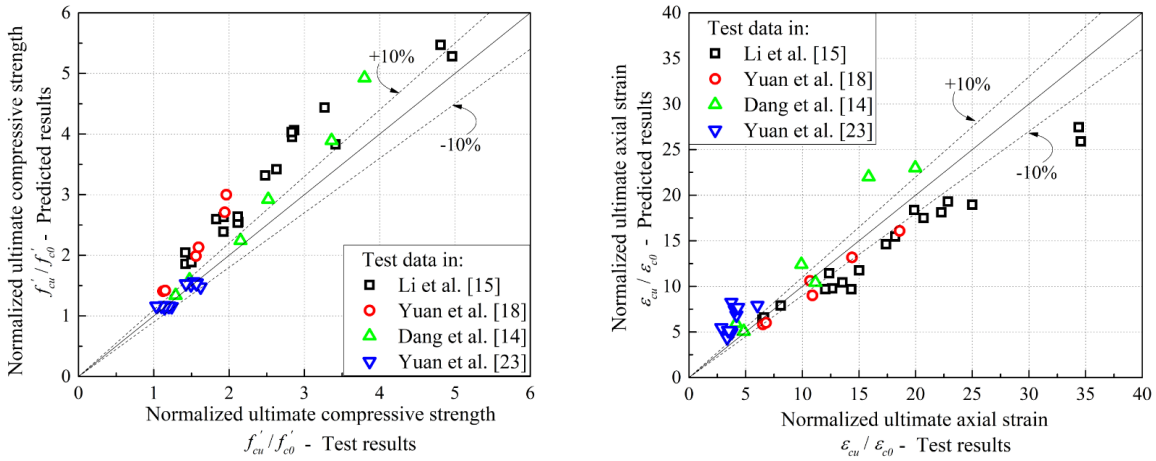

(a) Predictions by Teng et al.'s model [33]

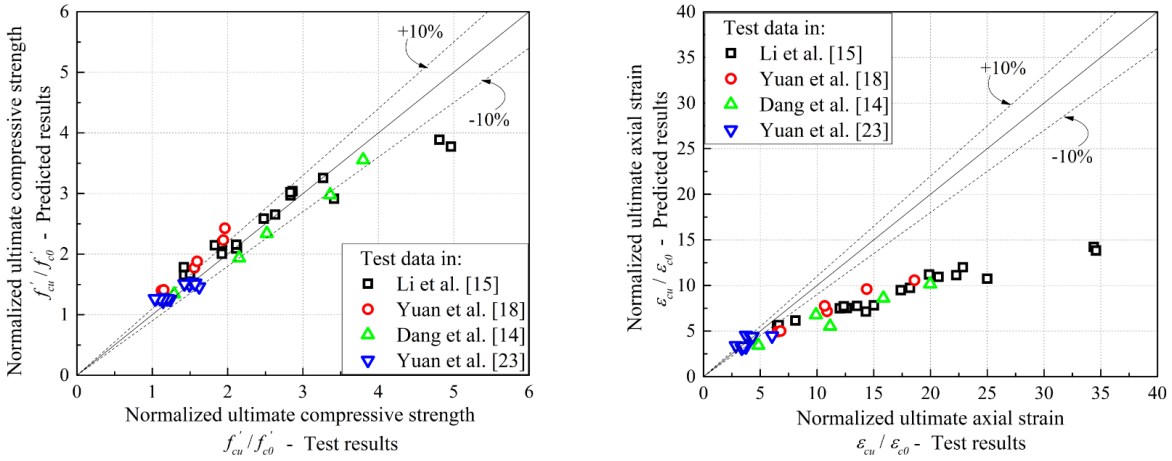

(b) Predictions by Wei and Wu's model [36]

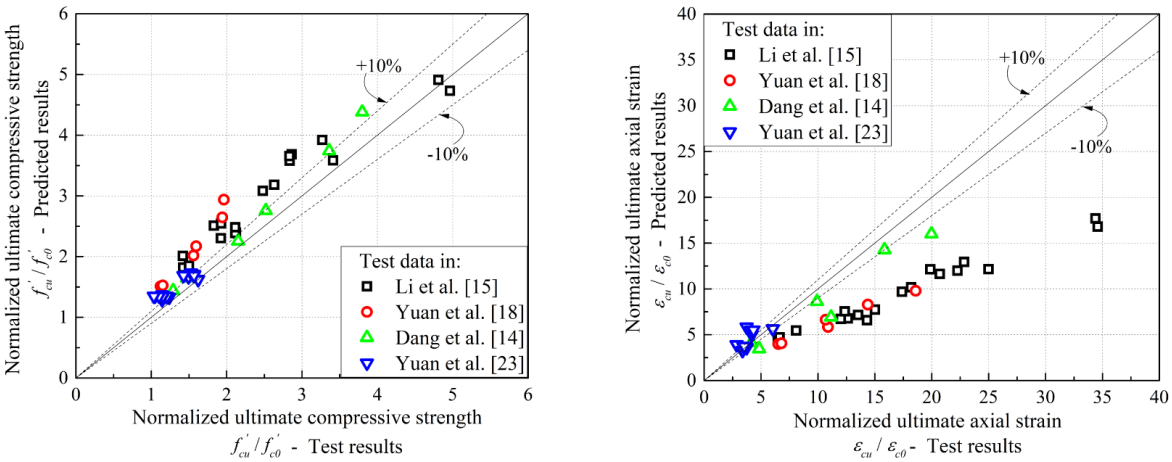

(c) Predictions by Ozbakkaloglu and Lim's model [37]

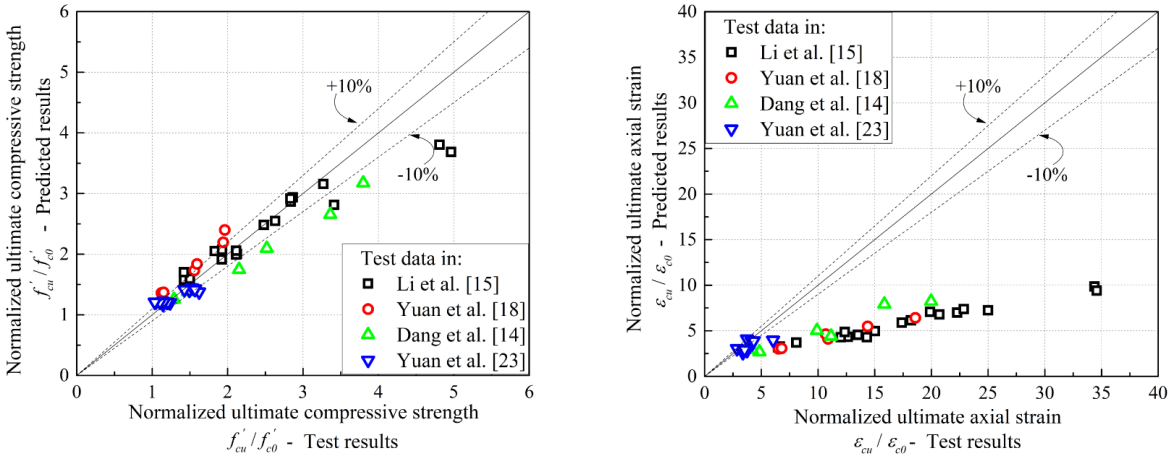

(d) Predictions by Pour et al.'s model [38]

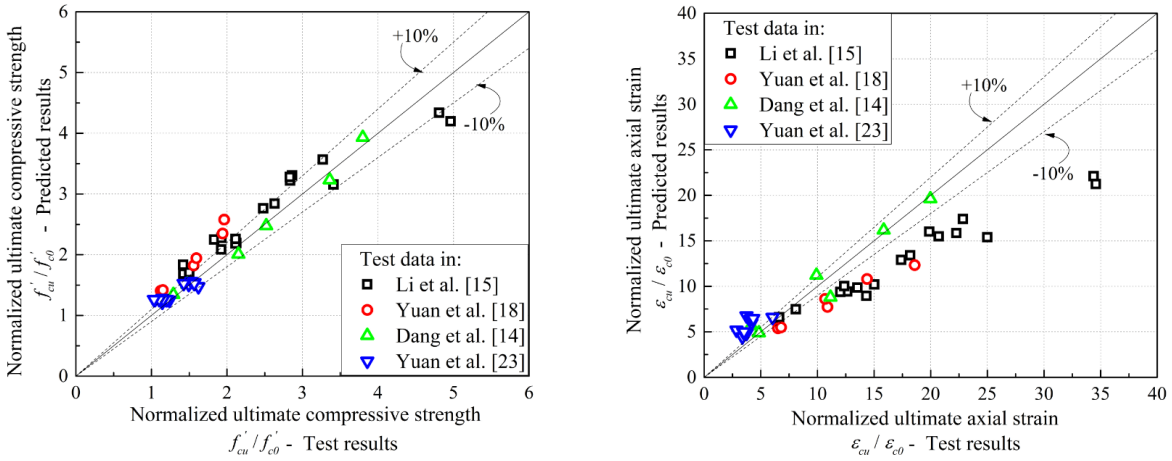

(e) Predictions by Dang et al.'s model [14]

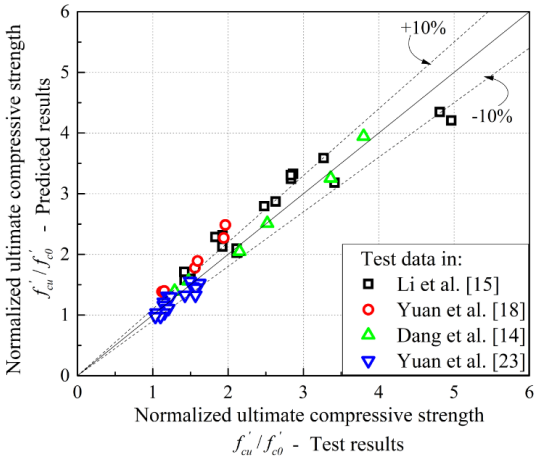

(f) Predictions by Yuan et al.'s model [23]

Fig. 4 Comparisons of ultimate conditions between test results and predicted results by existing design equations

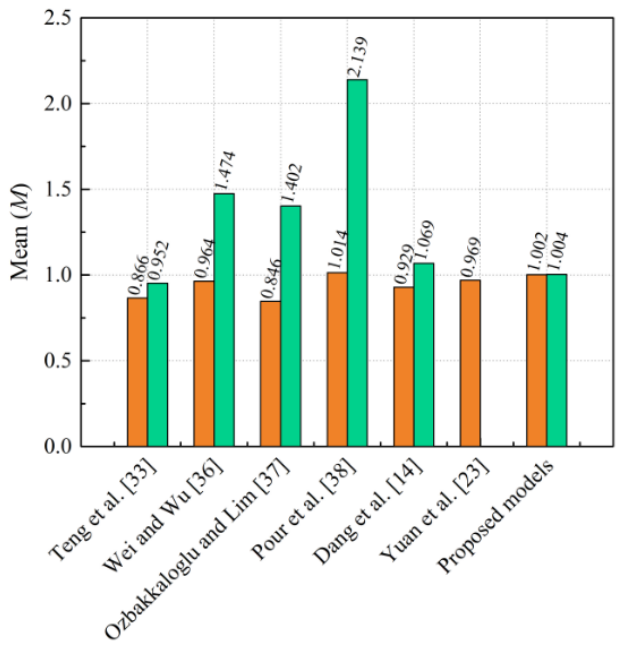

(a) Mean (M)

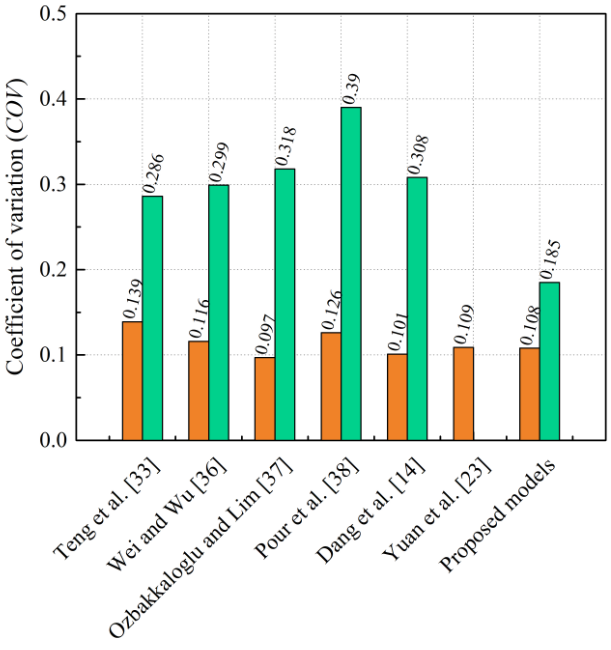

(b) Coefficient of variation (COV)

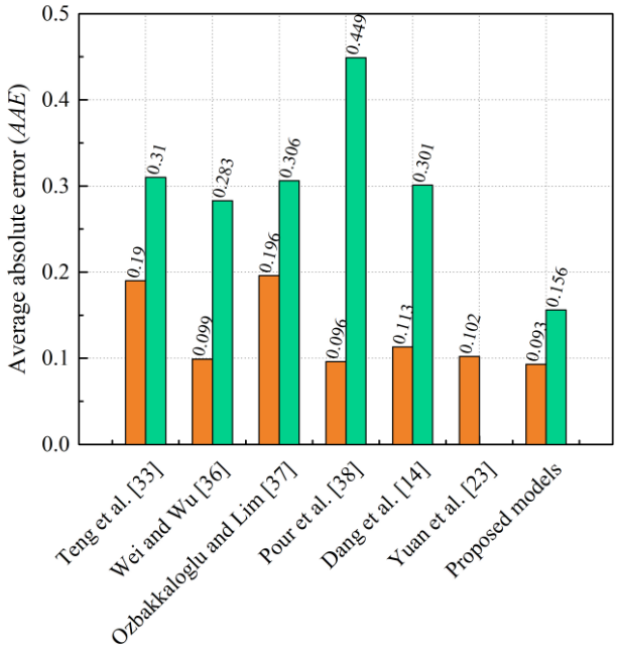

(c) Average absolute error (AAE)

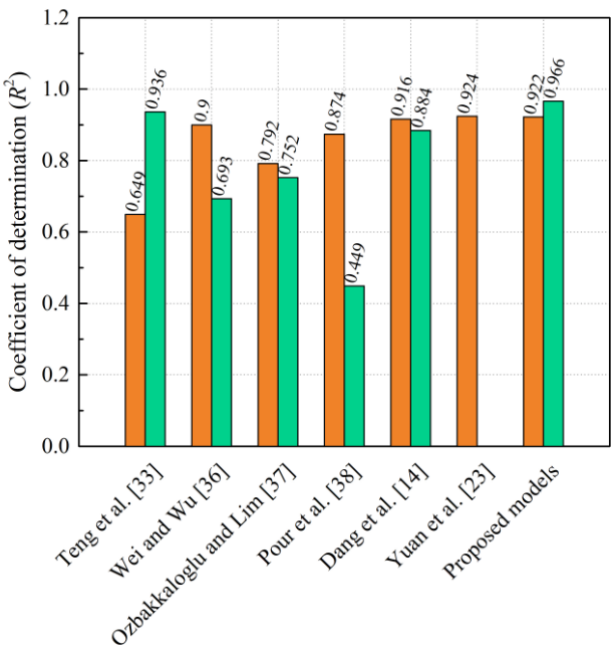

(d) Coefficient of determination (R^2)

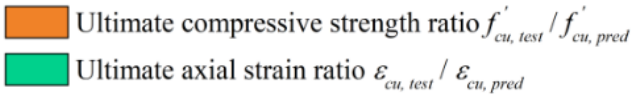

Fig. 5 Performance of different prediction models

As observed in Table 4 and Figs. 4 and 5, Dang et al. 's model [14] and Yuan et al.'s model [23] developed based on FRP-confined ECC perform better than the other models developed based on FRP-confined normal concrete in terms of both ultimate compressive strength and ultimate axial strain

predictions. However, Dang et al. 's model [14] and Yuan et al.'s model [23] can provide more accurate predictions for the data collected from their own research in *Refs*. [14] and [23], while the deviations are still relatively large for the data collected from other two literatures Li et al. [15] and Yuan et al. [18]. As mentioned in the Introduction of this paper, the reason that the models developed for FRP-confined normal concrete are not applicable to FRP-confined ECC is believed to be caused by the different mechanical properties between ECC and normal concrete under compression. It is reported in the literature that the lateral dilation of ECC can be restrained with the presence of fibers in the ECC mixture [14,15]. Under the same level of FRP-confinement, the hoop strain development of FRP-confined ECC is slower than that of FRP-confined normal concrete with the similar compressive strength [41-43]. Yuan et al. [18] also proposed the new dilation model that described the hoop strain-axial strain relation for FRP-confined ECC and performed better than those models developed based on FRP-confined normal concrete [44-46]. Therefore, it is important to develop the design model suitable for FRP-confined ECC, which will be presented in the following section of this paper.

4. New proposed design-oriented stress-strain model

In this section, design-oriented model for FRP-confined ECC is proposed. Design equations on ultimate conditions including ultimate compressive strength and ultimate axial strain are firstly developed. Stress-strain model that can describe the overall compressive behavior of FRP-confined ECC from the beginning to FRP rupture failure is then proposed.

4.1 Ultimate conditions

As presented in Table 3, the existing design equations relate the ultimate compressive strength f'_{cu} and ultimate axial strain ε_{cu} to confining pressure $f_{lu,a}$, confining stiffness K_l, confinement stiffness ratio ρ_K and strain ratio ρ_ε corresponding to FRP rupture. Based on Eqs. (1-3), the following relations can be derived:

$$\frac{f_{lu,a}}{f'_{c0}} = \frac{K_1 \varepsilon_{h,rup}}{f'_{c0}} = \rho_K \rho_\varepsilon \tag{10}$$

It indicates that the ultimate conditions for FRP-confined concrete can be directly related to confinement stiffness ratio ρ_K and strain ratio ρ_ε. Teng et al. [33] proposed the corresponding formula forms for ultimate compressive strength and ultimate axial strain as follows:

$$\frac{f'_{cu}}{f'_{c0}} = C_1 + k_1 f_1(\rho_K) g_1(\rho_\varepsilon) \tag{11}$$

$$\frac{\varepsilon_{cu}}{\varepsilon_{c0}} = C_2 + k_2 f_2(\rho_K) g_2(\rho_\varepsilon) \tag{12}$$

in which C_1 and C_2 are constants; k_1 and k_2 are enhancement coefficients of ultimate compressive strength and ultimate axial strain; $f_1(\rho_K)$ and $f_2(\rho_K)$ are functions of confinement stiffness ratio ρ_K and $g_1(\rho_\varepsilon)$ and $g_2(\rho_\varepsilon)$ are functions of strain ratio ρ_ε for ultimate compressive strength and ultimate axial strain, respectively. The formula forms presented in Eqs. (11) and (12) will be adopted to propose the design equations for the ultimate conditions of FRP-confined ECC in this study.

4.1.1 Ultimate axial strain

In Eq. (12), the constant C_2 reflects the ratio between the ultimate compressive strain ε_{cu} and the strain at peak stress ε_{c0} for unconfined concrete. For normal concrete with normal compressive strength, 0.002 and 0.0035 are generally taken as the values for ε_{c0} and ε_{cu} respectively [24], which yields $C_2 = 1.75$ [33,47]. Teng et al. [33] suggested that the constant C_2 can be adjusted to different values according to the different compressive properties of the plain concrete. When it comes to high strength concrete (HSC), ε_{cu} is normally equal to ε_{c0} since the brittleness of HSC will lead to the sudden failure at the peak point and no post peak stage can be obtained. Consequently, $C_2 = 1.0$ is taken in the design equations of ultimate axial strain for FRP-confined HSC as suggested by some literatures [48,49]. Meng et al. [50] and Li et al. [15] reported that the compressive behavior of unconfined ECC is different from that of unconfined normal concrete with similar compressive strength. For plain ECC

299 with normal compressive strength under compression, the stress will drop suddenly to maintain a
300 limited residual strength after reaching the peak stress, in comparison to that the stress will drop
301 gradually in the post-peak stage for the normal concrete counterpart. As suggested by Li et al. [21,22],
302 it can be conservatively considered that the ultimate compressive strain ε_{cu} is equal to the strain at
303 peak stress ε_{c0} for ECC with no FRP confinement, indicating $C_2 = 1.0$ in Eq. (12).

304 Based on the collected test data, the following equation can be obtained by regression:

305 $$\frac{\varepsilon_{cu}}{\varepsilon_{c0}} = 1 + 21\rho_K^{0.98}\rho_\varepsilon^{1.02} \quad (13)$$

306 Close agreements of ultimate axial strain between the test results and predicted results by Eq. (13) can
307 be noted as shown in Fig. 6. Statistical indicators calculated using Eqs. (6-9) for the proposed Eq. (13)
308 are presented in Table 4 and in Fig. 5. Compared with the other existing models, more accurate
309 predictions can be generated by Eq. (13) with much lower *COV* and *AAE* values and *M* and R^2 values
310 closer to 1. It is worth noting that three test data from Dang et al. [14] have the largest deviations with
311 the predicted results as shown in Fig. 6. In *Ref.* [15], when the test stress-strain curves from Dang et
312 al. [14] were compared with the predictions by the proposed analysis-oriented model, relatively large
313 deviations were observed as well, followed by the discussion of possible reasons. The similar reasons
314 are believed to cause the deviations here with the prediction by Eq. (13). Detailed information can be
315 referred to *Ref.* [15].

316

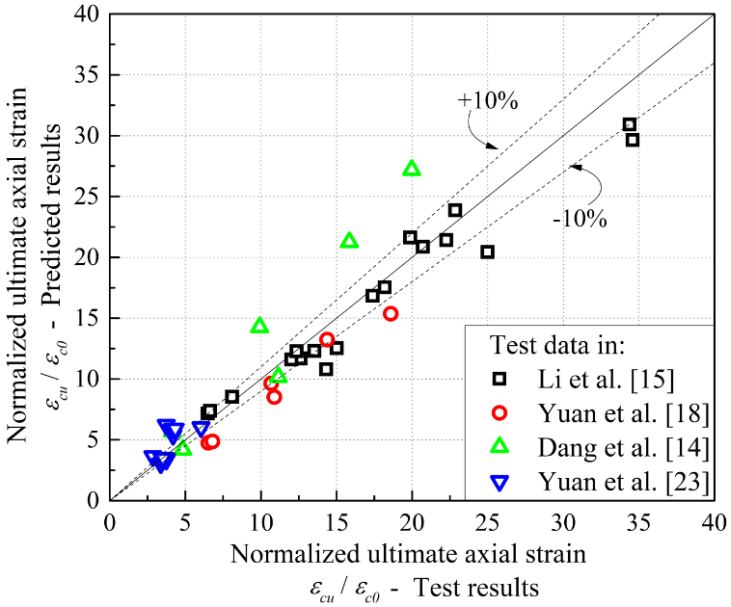

317

318 Fig. 6 Comparisons of ultimate axial strain between test results and predicted results with proposed

319 equation Eq. (13)

320 4.1.2 Ultimate compressive strength

321 The function format as shown in Eq. (11) will be used for the equation of ultimate compressive strength

322 of FRP-confined ECC. $C_1 = 1.0$ will be adopted to consider that the ultimate compressive strength is

323 equal to the peak stress for unconfined ECC. Lam and Teng [47] reported that the axial stress-axial

324 strain curve and axial stress-lateral strain curve for FRP-confined concrete exhibit the bilinear relation

325 with two linear portions connected by a smooth transition zone. It was also noted by Teng et al. [33]

326 that the second portion of the axial stress-lateral strain curve is closer to a straight line which intersects

327 with the axial stress axis at the unconfined concrete strength, compared to that of the axial stress-axial

328 strain curve. Therefore, the following expression was adopted by Teng et al. [33] for the compressive

329 stress of FRP-confined concrete σ_c in the second linear portion:

330 $$\frac{\sigma_c}{f'_{c0}} = 1 + K\frac{\varepsilon_l}{\varepsilon_{c0}} \quad (14)$$

331 in which K is the slope of the straight line(second linear portion) and is related to confinement stiffness

332 ratio ρ_K. For the ultimate compressive strength at FRP rupture, $\varepsilon_l = \varepsilon_{h,rup}$ and it yields:

$$\frac{f'_{cu}}{f'_{c0}} = 1 + K\frac{\varepsilon_{h,rup}}{\varepsilon_{c0}} = 1 + K\rho_{\varepsilon} \quad (15)$$

Recently, Li et al. [15] proposed the first analysis-oriented model for FRP-confined ECC. This model has been validated with test results obtained from their own and other researchers, which are covered by the database in the current study as presented in Table. 1. With this analysis-oriented model, full stress-strain curves of FRP-confined ECC can be generated with iteration steps. Fig. 7(a) presents the generated curves of normalized axial stress σ_c/f'_{c0} versus normalized lateral strain $\varepsilon_l/\varepsilon_{c0}$ for ECC with the compressive strength of 30 MPa under different levels of FRP confinement. Linear fitting with the equation format as expressed in Eq. (14) is generated for the second portion as shown in Fig. 7(a). As suggested by Teng et al. (2009), $\varepsilon_l/\varepsilon_{c0} = 0.5$ is set as the starting point of the second portion for different curves. The fitted lines are all ensured to intersect the axial stress axis at unit 1.0. However, it can be noted that the fitted line cannot accurately capture the second portion of the axial stress-lateral strain curve in the range of $\varepsilon_l/\varepsilon_{c0} = 0.5$ and onwards. With the increase of confining stiffness, the difference of the slope between the fitted line and the axial stress-lateral strain curve becomes more obvious. The reason is that the second portion ($\varepsilon_l/\varepsilon_{c0} = 0.5$ and onwards) in the axial stress-lateral strain curve still presents slightly nonlinear behavior, which leads to that the linear Eq. (14) cannot generate accurate prediction. Therefore, it also indicates that f'_{cu} is not linearly related to ρ_{ε} and Eq. (15) could not accurately predict the ultimate compressive strength of FRP-confined ECC.

Power function is adopted for normalized lateral strain $\varepsilon_l/\varepsilon_{c0}$ and the same set of curves in Fig. 7(a) are regenerated by changing the horizontal axis from $\varepsilon_l/\varepsilon_{c0}$ to $(\varepsilon_l/\varepsilon_{c0})^m$ as shown in Fig. 7(b), in which the parameter m is adopted as the index in the power function. Linear fittings are adopted for the second portion of the curves starting from $\varepsilon_l/\varepsilon_{c0} = 0.5$. The values of m are adjusted for each curve to ensure that the intercepts of the fitted lines are equal to 1.0 as well as the slope of the fitted line fully capture that of the second portion of the modified stress-strain curve, as illustrated in Fig. 7(b). A parametric study was conducted with the analysis-oriented model of FRP-confined ECC (Li et

al. [15]) and the aforementioned fitting approach. Material properties of ECC and FRP covered in the parametric study are presented in Table 5. Diameter of the ECC cylinder is 150 mm. Hoop rupture strains of GFRP and CFRP adopt the same values as those in Teng et al. [33]. The relation between parameter m and confinement stiffness ratio ρ_K is shown in Fig. 7(c). It is observed that with the increase of ρ_K, m increases firstly at lower confining stiffness level and then converges to the value of around 0.9. Overall, m is in the range of the 0.77 – 0.91 for the current parametric study as presented in Table 5. To simplify the design equation, m is considered to be independent on ρ_K and $m = 0.9$ is adopted as the index in the power function of $(\varepsilon_l/\varepsilon_{c0})^m$. Meanwhile, the relation between K, which is the slope of the fitted lines in Fig. 7(b), and ρ_K is shown in Fig. 7(d). It is noted that K is highly linear related to ρ_K, with the following regressed expression:

$$K = 2.9(\rho_K - 0.01) \tag{16}$$

Therefore, the equation for predicting the ultimate compressive strength of FRP-confined ECC can be proposed as follows:

$$\frac{f'_{cu}}{f'_{c0}} = 1 + 2.9(\rho_K - 0.01)(\rho_\varepsilon)^{0.9} \tag{17}$$

Comparing Eq. (17) with Teng et al.'s expression [33], which is a widely accepted design model for FRP-confined normal concrete (especially with normal compressive strength), the following characteristics can be noted: (1) the strength enhancement factor is modified from 3.5 to 2.9; (2) the threshold of confinement stiffness ratio for effective confinement is remained to be 0.01; (3) linear function of ρ_ε is replaced with power function of $(\rho_\varepsilon)^{0.9}$. It also reflects the similarities and differences between the design prediction equations for FRP-confined normal concrete and FRP-confined ECC. Comparisons between test results and predicted results is presented in Fig. 8. The close agreement indicates the good performance of the Eq. (17) on predicting the ultimate compressive strength of FRP-confined ECC. Statistical indicators calculated using Eqs. (6-9) for the proposed Eq. (17) are presented in Table 4 and in Fig. 5. Compared with the other existing models, more accurate predictions can be

generated using Eq. (17). It is worth noting that the general process used to develop the equation for ultimate compressive strength was based on the approach initially proposed by Teng et al. [33], while power function of $(\varepsilon_l/\varepsilon_{c0})^m$ was further incorporated for better prediction results.

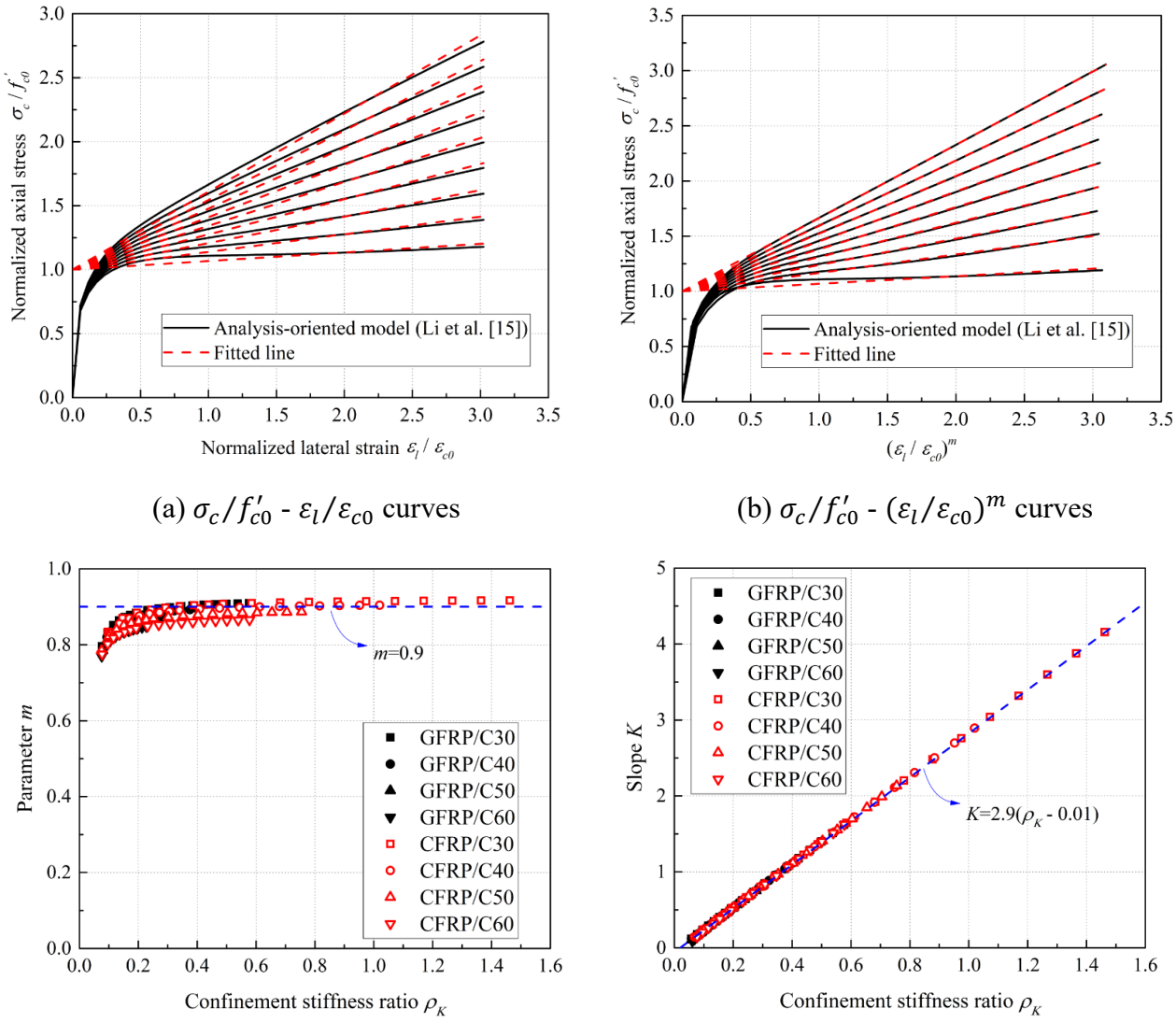

(a) σ_c/f_{c0}' - $\varepsilon_l/\varepsilon_{c0}$ curves

(b) σ_c/f_{c0}' - $(\varepsilon_l/\varepsilon_{c0})^m$ curves

(c) Relations between m and ρ_K

(d) Relations between K and ρ_K

Fig. 7 Demonstration of the parametric study with the analysis-oriented model

Table 5 Material properties covered in the parametric study

ECC	f'_{c0} (MPa)	30, 40, 50, 60
	ε_{c0}	Eq. (4)
	E_c (MPa)	Eq. (5)
GFRP	E_f (GPa)	100.5
	t_f (mm)	0-3 at an interval of 0.2
	$\varepsilon_{h,rup}$	0.015
CFRP	E_f (GPa)	255
	t_f (mm)	0-3 at an interval of 0.1
	$\varepsilon_{h,rup}$	0.0075

Note: The values of modulus of elasticity of GFRP and CFRP are kept the same as those in Yuan et al. [18] and Li et al. [15].

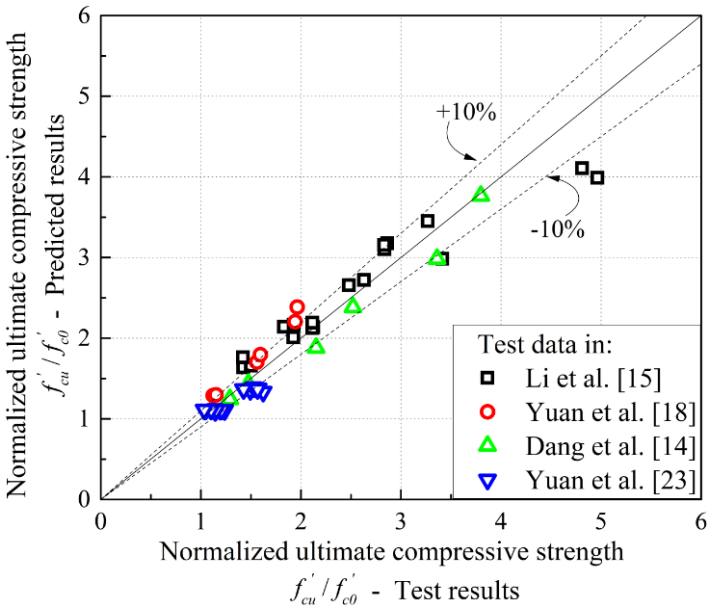

Fig. 8 Comparisons of ultimate compressive strength between test results and predicted results with proposed equation Eq. (17)

4.2 Stress-strain model

In order the predict the overall compressive behavior of FRP-confined ECC, stress-strain model is proposed in this section. Lam and Teng's model [47] has been widely used for FRP-confined normal concrete. Since the typical compressive stress-strain curves for FRP-confined normal concrete and FRP-confined ECC are similar, Lam and Teng's model [47] can be adopted for the design model of

406 FRP-confined ECC with the corresponding replacement of the prediction equations of the ultimate
407 conditions as introduced in Section 4.1 of this paper. Lam and Teng's model [47] defines the
408 compressive stress-strain curve ($\sigma_c - \varepsilon_c$) as a first parabolic portion and a second linear portion with
409 smooth transition in between, as illustrated in Fig.9. According to the definition of design-oriented
410 model for FRP-confined concrete in Ozbakkaloglu et al. [51], it belongs to the model with type IIIb
411 curve. Lam and Teng's design-oriented model [47] is expressed as follows:

412 $$\sigma_c = \begin{cases} E_c\varepsilon_c - \frac{(E_c - E_2)^2}{4f'_{c0}}\varepsilon_c^2 & (0 \le \varepsilon_c \le \varepsilon_t) \\ f'_{c0} + E_2\varepsilon_c & (\varepsilon_t < \varepsilon_c \le \varepsilon_{cu}) \end{cases} \quad (18)$$

413 where f'_{c0} and E_c are unconfined compressive strength and elastic modulus of concrete. E_2 and ε_t are
414 the slope of the second linear portion and the transition strain between the first parabolic portion and
415 the second linear portion, with the following expressions:

416 $$E_2 = \frac{f'_{cu} - f'_{c0}}{\varepsilon_{cu}} \quad (19)$$

417 $$\varepsilon_t = \frac{2f'_{c0}}{E_c - E_2} \quad (20)$$

418 f'_{cu} and ε_{cu} are the ultimate compressive strength and ultimate axial strain and can be determined by
419 Eq. (17) and Eq. (13), respectively. Comparisons between test stress-strain curves and predicted stress-
420 strain curves are presented in Fig. 10. Close agreements demonstrate the good performance of Lam
421 and Teng's model [47] incorporating the proposed equations of ultimate conditions for the prediction
422 of the overall compressive behavior of FRP-confined ECC. It is worth noting that Lam and Teng's
423 model [47] may not be suitable for FRP-confined high strength concrete, especially when the FRP
424 confinement is not sufficient. In future studies, more comprehensive design-oriented model for FRP-
425 confined ECC with both normal strength and high strength could be developed using database on FRP-
426 confined ECC with larger range of ECC strength and under various confinement levels. Meanwhile,
427 the proposed design-oriented model was developed and validated by the collected test data in the

database for FRP-confined ECC in this paper. The database was assembled by the available test data in the current existing literature. Only conventional GFRP and CFRP were included as the confining material, while GFRP was used for most of the specimens. Therefore, the proposed model may only be applicable to GFRP and CFRP-confined ECC (especially GFRP-confined ECC) in the current scope of this study due to the limited test data. More tests on confined ECC with various FRP confining materials could be conducted to generate new data for further validation of the proposed design-oriented model in future studies.

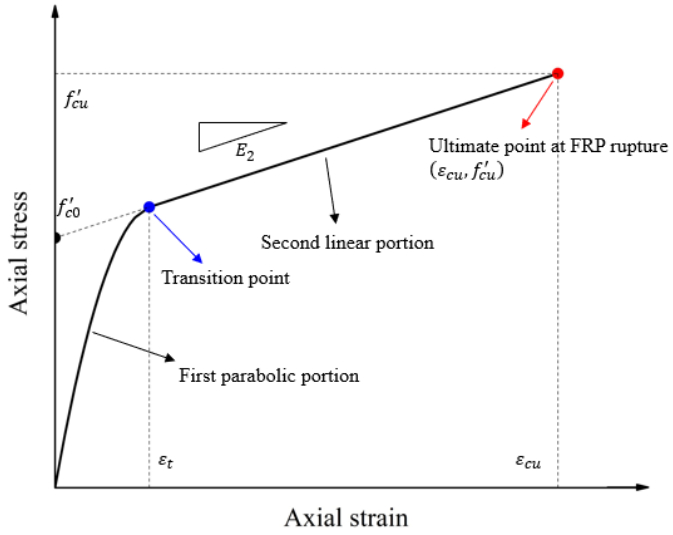

Fig. 9 Design-oriented stress-str ain model for FRP-confined concrete

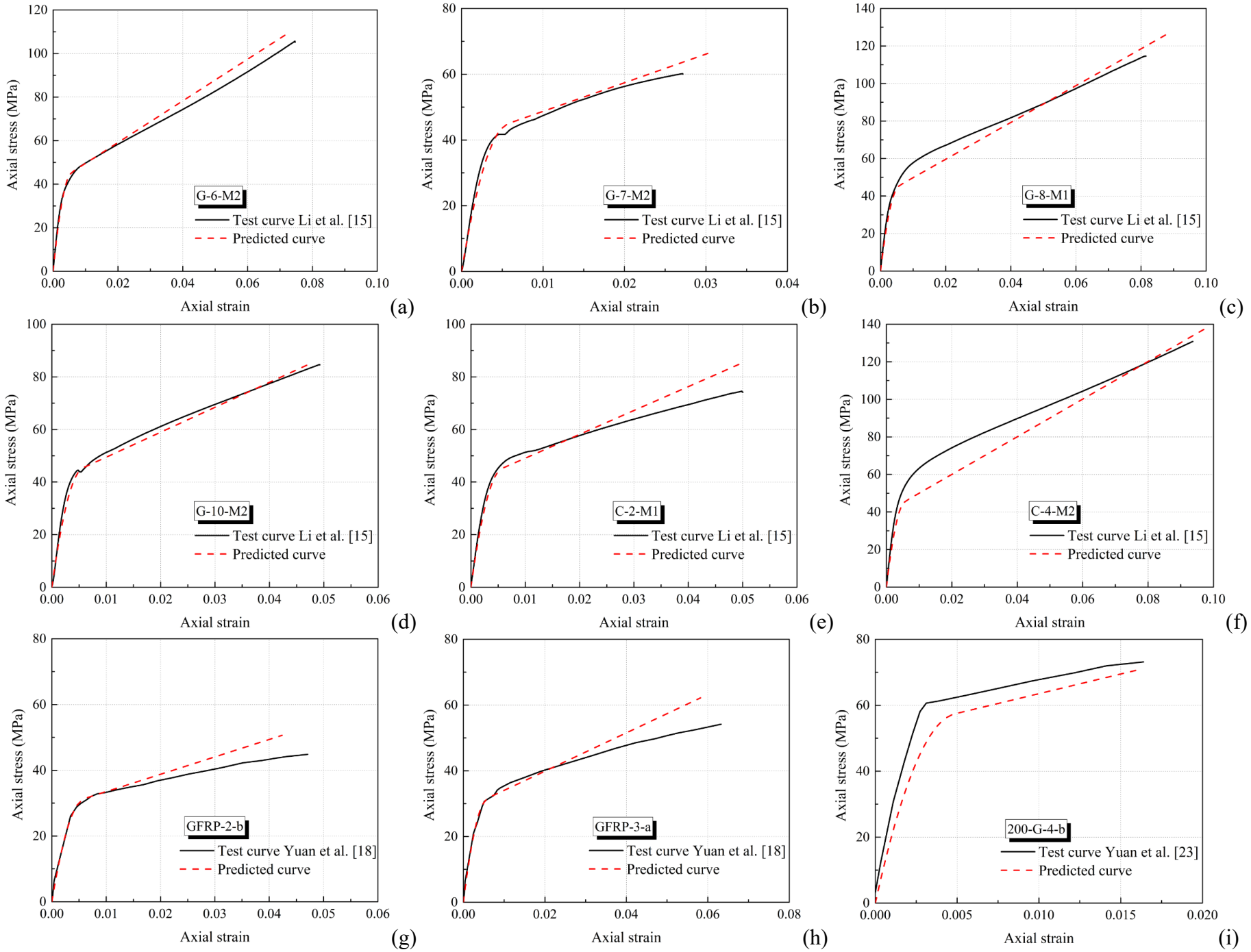

Fig. 10 Comparisons of compressive stress-strain curves between test results and predicted results for FRP-confined ECC

5. Conclusions

This paper presents the investigation on FRP-confined engineered cementitious composites (ECC) and aims to propose the corresponding design recommendation. A test database for FRP-confined ECC was first collected from the literature. The existing design equations, including those developed for FRP-confined normal concrete and FRP-confined ECC, were evaluated. New equations for ultimate conditions were developed and incorporated into Lam and Teng's stress-strain model [47] to form the new design-oriented model for FRP-confined ECC. Detailed conclusions can be drawn from the current study as follows:

(1) The representative equations of elastic modulus and compressive strain at the peak stress for plain normal concrete are not applicable to plain ECC, which reflects the different mechanical properties between these two cementitious materials. It is caused by the absence of coarse aggregates and presence of short fibers in ECC.

(2) The existing equations developed for FRP-confined normal concrete could not provide accurate predictions on the ultimate conditions of FRP-confined ECC. In general, they overestimate the predictions of ultimate compressive strength while underestimate the predictions of the ultimate axial strain. These observations also demonstrate the different confinement effectiveness, strength and strain enhancements between FRP-confined normal concrete and FRP-confined ECC.

(3) New equation for ultimate axial strain was developed through regression of the collected test data and presented the closer agreements with test results in comparison to the other existing models, with the statistical performance of $M = 1.004$, $COV = 0.185$, $AAE = 0.156$ and $R^2 = 0.966$. New equations for ultimate compressive strength were developed based on the analysis-oriented model for FRP-confined ECC and the corresponding parametric studies. It showed close agreements in comparison to test results with $M = 1.002$, $COV = 0.108$, $AAE = 0.093$ and $R^2 = 0.922$.

(4) The new developed equations of ultimate conditions were adopted in Lam and Teng's model [47] to form the design-oriented model for FRP-confined ECC. The generated stress-strain curve agreed well with the test curves, which indicates the good performance of the new design-oriented stress-strain model in predicting the overall compressive behavior of FRP-confined ECC.

CRediT authorship contribution statement

Shuai Li: Investigation, Writing - original draft. **Tak-Ming Chan:** Writing - review & editing, Funding acquisition, Supervision. **Ben Young:** Writing - review & editing, Funding acquisition, Supervision.

Declaration of Competing Interest

The authors declare that they have no known competing financial interests or personal relationships that could have appeared to influence the work reported in this paper.

Acknowledgement

The research work presented in this paper was supported by the Research Grants Council of the Hong Kong Special Administrative Region, China – Theme-based Research Scheme (Project No. T22-502/18-R).

References

[1] Li VC. On engineered cementitious composites (ECC). J Adv Concr Technol 2003;1 (3):215–30.

[2] Xu LY, Huang BT, Li VC, Dai JG. High-strength high-ductility Engineered/Strain-Hardening Cementitious Composites (ECC/SHCC) incorporating geopolymer fine aggregates. Cem Concr Compos 2022;125:104296.

[3] Huang BT, Wu JQ, Yu J, Dai JG, Leung CKY, Li VC. Seawater sea-sand engineered/strain-hardening cementitious composites (ECC/SHCC): Assessment and modeling of crack characteristics. Cem Concr Res 2021;140:106292.

[4] Li VC, Wang S, Wu C. Tensile strain-hardening behavior of polyvinyl alcohol engineered cementitious composite (PVA-ECC). ACI Mater J 2001;98(6):483–92.

[5] Zhu JX, Xu LY, Huang BT, Weng KF, Dai JG. Recent developments in Engineered/Strain-Hardening Cementitious Composites (ECC/SHCC) with high and ultra-high strength. Constr Build Mater 2022;342:127956.

[6] Liao JC, Xu LY, Huang BT, Dai JG, Shah SP. Strain-hardening Ultra-High-Performance Geopolymer Concrete (UHPGC): Matrix design and effect of steel fibers. Compos Commun 2022;30:101081.

[7] Qin F, Zhang Z, Yin Z, Di J, Xu L, Xu X. Use of high strength, high ductility engineered cementitious composites (ECC) to enhance the flexural performance of reinforced concrete beams. J Build Eng 2020;32:101746.

[8] Yang X, Gao WY, Dai JG, Lu ZD, Yu KQ. Flexural strengthening of RC beams with CFRP grid-reinforced ECC matrix. Compos Struct 2018;189:9-26.

[9] Al-Gemeel AN, Zhuge Y. Using textile reinforced engineered cementitious composite for concrete columns confinement. Compos Struct 2019;210:695-706.

[10] Zeng JJ, Liang QJ, Cai WJ, Liao J, Zhou JK, Zhu JY, Zhang L. Strengthening RC square columns with UHP-ECC section curvilinearization and FRP confinement: Concept and axial compression tests. Eng Struct;2023:115666.

[11] Lee CK, Khan MKI, Zhang YX, Rana MM. Compressive performance of ECC-concrete encased high strength steel composite columns. Eng Struct 2020;213:110567.

[12] Li X, Li Y, Yan M, Meng W, Lu X, Chen K, Bao Y. Cyclic behavior of joints assembled using prefabricated beams and columns with Engineered Cementitious Composite (ECC). Eng Struct 2021;247:113115.

[13] Dong B, Pan J, Cai J, Xu L. Mechanical behaviour of a new ECC-encased CFST column to RC beam connection under cyclic loading. Eng Struct 2021;234:111915.

[14] Dang Z, Feng P, Yang JQ, Zhang Q. Axial compressive behavior of engineered cementitious composite confined by fiber-reinforced polymer. Compos Struct 2020;243:112191.

[15] Li S, Chan T-M, Young B. Compressive behavior and analysis-oriented model of FRP-confined engineered cementitious composite columns. Eng Struct 2022;270:114869.

[16] Lam L, Teng JG, Cheung CH, Xiao Y. FRP-confined concrete under axial cyclic compression. Cem Concr Compos 2006;28(10):949–58.

[17] Lam L, Teng JG. Stress–strain model for FRP-confined concrete under cyclic axial compression. Eng Struct 2009;31:308–21.

[18] Yuan WY, Han Q, Bai YL, Du XL, Yan ZW. Compressive behavior and modelling of engineered cementitious composite (ECC) confined with LRS FRP and conventional FRP. Compos Struct 2021;272:114200.

[19] Li S, Chan T-M, Young B. Experimental investigation on axial compressive behavior of novel FRP-ECC-HSC composite short column. Compos Struct 2023;303:116285.

[20] Li S, Chan T-M, Young B. Mechanical analysis and finite element modeling of FRP-ECC-HSC composite stub column under axial compression. J Build Eng 2022;62:105212.

[21] Li S, Chan T-M, Young B. Behavior of GFRP-concrete double tube composite columns. Thin Walled Struct 2022;178:109490.

[22] Li S, Chan T-M, Young B. Cyclic compressive behavior and load–strain model of FRP-concrete double tube composite columns. Thin Walled Struct 2023;184:110515.

[23] Yuan WY, Han Q, Bai YL, Song YC, Zhang Q. Size effect on compressive behavior of FRP-confined engineered cementitious composites (ECC). Constr Build Mater 2022;348:128610.

[24] CEN. Eurocode 2: Design of concrete structures – Part 1-1: General rules for buildings. EN 1993-1-1, European Committee for Standardization (CEN), Brussels, 2004.

[25] Architectural Institute of Japan (AIJ). AIJ standard for Structural Calculation of Reinforced Concrete Structures Revised 2018; AIJ: Tokyo, Japan, 2018.

[26] ACI 318 Committee. Building Code Requirements for Structural Concrete (ACI 318-19) and Commentary; American Concrete Institute: Farmington Hills, MI, USA, 2019.

[27] Popovics S. A numerical approach to the complete stress-strain curve of concrete. Cem Concr Res 1973;3:583–99.

545 [28] Lim JC, Ozbakkaloglu T. Unified stress-strain model for FRP and actively confined normal-
546 strength and high-strength concrete. J Compos Constr 2015;19)4):04014072.

547 [29] Tasdemir MA, Tasdemir C, Akyuz S, Jefferson AD, Lydon FD, Barr BIG. Evaluation of strains
548 at peak stresses in concrete: A three-phase composite model approach. Cem Concr Compos
549 1998;20:301-318.

550 [30] De Nicolo, B., Pani, L, Pozzo, E. Strain of concrete at peak compressive stress for a wide range
551 of compressive strengths. Materials and Structures 1994;27:206–210.

552 [31] Zhou J, Pan J, Leung CKY. Mechanical behavior of fiber reinforced engineered cementitious
553 composites in uniaxial compression. J Mater Civ Eng 2015;27(1):04014111.

554 [32] Ding Y, YU K, Mao W. Compressive performance of all-grade engineered cementitious
555 composites: Experiment and theoretical model. Constr Build Mater 2020;244:118357.

556 [33] Teng JG, Jiang T, Lam L, Luo YZ. Refinement of a design-oriented stress–strain model for FRP-
557 confined concrete. J Compos Constr 2009;13(4):269–78.

558 [34] Concrete Society. Design guidance for strengthening concrete structures with fibre composite
559 materials. Technical Rep. No. 55, 3rd Ed., Crowthorne, Berkshire, U.K. 2012.

560 [35] American Concrete Institute ACI. Guide for the design and construction of externally bonded
561 FRP systems for strengthening concrete structures. ACI-440 2R, Farmington Hills, Mich. 2017.

562 [36] Wei YY, Wu YF. Unified stress-strain of concrete for FRP-confined columns. Constr Build Mater
563 2012;26:381-392.

564 [37] Ozbakkaloglu T, Lim JC. Axial compressive behavior of FRP-confined concrete: Experimental
565 test database and a new design-oriented model. Compos Part B 2013;55:607-634.

566 [38] Pour AF, Ozbakkaloglu T, Vincent T. Simplified design-oriented axial stress-strain model for
567 FRP-confined normal- and high-strength concrete. Eng Struct 2018;175:501-516.

568 [39] Zhu JY, Lin G, Teng JG, Chan T-M, Zeng JJ, Li LJ. FRP-Confined square concrete columns with
569 section curvilinearization under axial compression. J Compos Constr 2020;24 (2):04020004.

570 [40] Zhang B, Yu T, Teng JG. Behavior of concrete-filled FRP tubes under cyclic axial compression.
571 J Compos for Constr 2015;19(3):04014060.

572 [41] Teng JG, Huang YL, Lam L, Ye LP. Theoretical model for fiber-reinforced polymer-confined
573 concrete. J Compos Constr, 2007;11(2):201-210.

574 [42] Yang J, and Feng P. Analysis-oriented models for FRP-confined concrete: 3D interpretation and
575 general methodology. Eng Struct 2020;216:110749.

576 [43] Lim JC, and Ozbakkaloglu T. Lateral strain-to-axial strain relationship of confined concrete. J
577 Struct Eng 2015;141(5):04014141.

578 [44] Jiang T, Teng JG. Analysis-oriented stress–strain models for FRP–confined concrete. Eng Struct
579 2007;29(11):2968–86.

580 [45] Bai YL, Dai JG, Lin G, Mohammadi M. Stiffness-based design-oriented compressive stress-strain
581 model for large-rupture-strain (LRS) FRP-confined concrete. Compos Struct 2019;223:110953.

582 [46] Dai JG, Bai YL, Teng JG. Behavior and modeling of concrete confined with FRP composites of
583 large deformability. J Compos Constr 2011;15(6):963–73.

584 [47] Lam L, Teng JG. Design-oriented stress-strain model for FRP-confined concrete. Constr Build
585 Mater 2003;17(6):471–89.

586 [48] Cui C, Sheikh SA. Analytical model for circular normal- and high-strength concrete columns
587 confined with FRP. J Compos Constr 2010;14:562–72.

588 [49] Liao J, Zeng JJ, Gong QM, Quach WM, Gao WY, Zhang L. Design-oriented stress–strain model
589 for FRP-confined ultra-high performance concrete (UHPC). Constr Build Mater 2022;318:126200.

590 [50] Meng D, Huang T, Zhang YX, Lee CK. Mechanical behaviour of a polyvinyl alcohol fibre
591 reinforced engineered cementitious composite (PVA-ECC) using local ingredients. Constr Build
592 Mater 2017;141:259–70.

593 [51] Ozbakkaloglu T, Lim JC, Vincent T. FRP-confined concrete in circular sections: Review and
594 assessment of stress–strain models. Eng Struct 2013;49:1068-1088.